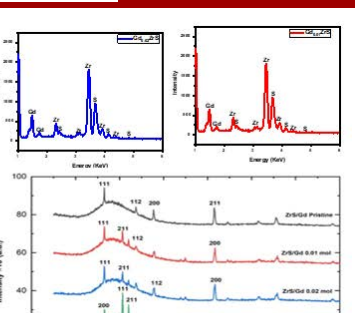
### Structural, optical and electrical properties evaluation of Gadoliniumdoped Zirconium Sulphide (ZrS/Gd) Thin Films prepared via electrostatic spray deposition for photonic and optoelectronic applications

Cletus Olisenekwu,1\* Samuel Oghenemega Shaka,2 Enoh Pius Ogherohwo,1 Oyibo Dafe Precious,1 Ikoko Precious<sup>1</sup>

<sup>1</sup>Department of Physics, Federal University of Petroleum Resources, Effurun, Nigeria. <sup>2</sup>Department of Science Laboratory Technology, Delta State University, Abraka. Nigeria.

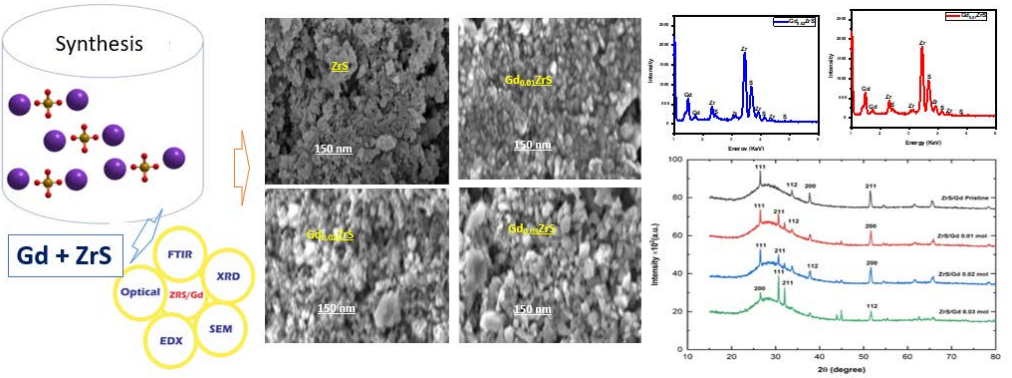
Submitted on: 14-May-2025, Revised: 03-Jul-2025, Accepted on: 04-Jul-2025, and Published on: 07-Jul-2025



Article

### ABSTRACT

This study investigates the synthesis and characterization of Gadolinium-doped Zirconium Sulphide (ZrS/Gd) thin films via Electrostatic Spray Deposition (ESD) for optoelectronic and photonic uses. Films were prepared at Gd concentrations of 0.01, 0.02, and 0.03 mol and



evaluated for their optical, electrical, and structural properties. UV-Vis analysis showed strong absorbance between 300-400 nm, peaking at 0.75 a.u for 0.01 mol. Bandgap values, derived from Tauc plots, increased from 3.19 eV (pristine) to 3.33 eV at 0.01 and 0.03 mol, while 0.02 mol showed 3.06 eV. Optical conductivity reached ~0.75 S/m, and the refractive index peaked near 3.8 eV photon energy. Electrical measurements revealed improved conductivity from 1.65 S/m (pristine) to 1.85 S/m, with corresponding resistivity decreasing from 0.61  $\Omega$ -m to 0.54  $\Omega$ -m at increased dopant molarity and thickness. XRD analysis showed increased crystallite size and reduced dislocation density, while SEM revealed uniform surface morphology with agglomerated nanoparticles. These findings confirm that Gd doping improves optical transparency, electrical conductivity, and structural integrity of ZrS thin films, suggesting strong potential for use in UV photodetectors, multicolour LEDs, solar-blind sensors, advanced display technologies, and other optoelectronics applications.

Keywords: Gadolinium, Zirconium-Sulphide, Electrostatic-Spray, Optoelectronics, Bandgap, Thin film, Characterization

### INTRODUCTION

Due to the improved physical and chemical characteristics of electronic nanoparticles over bulk materials, interest in these nanoparticles has skyrocketed in recent decades.<sup>1-4</sup> Numerous cutting-edge applications in the fields of medicine, pharmacy, electronics, agriculture, solid state and material science, the food industry, and many more have been made possible by these exceptional qualities. 4-6 Chalcogenides are semiconductors with a narrow band gap that are frequently employed as photocatalysts. 7,8 For photonics, optoelectronics, microelectronics, and plasma-electronics applications, these narrow-band gap materials enable more effective absorption of more than 40% of solar energy in visible light, thereby enhancing their photo-catalytic and electrical capabilities. 9-12 These materials produce electron and hole (e-/h+) pairs when exposed to visible light. 13 Nanomaterials based on chalcogenides are widely recognized for their significant uses. Due to their narrow band gap energy, visible light harvesting capability, and numerous applications such as solar energy utilization, visible light-induced photocatalysis, visible light-assisted water splitting, optoelectronic devices, and hazardous pollutant removal, chalcogenide nanostructures have drawn the interest of researchers.14

Gadolinium (Gd, atomic mass 157.25, atomic number 64), a soft silvery-white metal that interacts with water and oxygen. Gadolinium has seven unpaired electrons in its ionic trivalent form, which results in a significant intrinsic magnetic moment.

\*Corresponding Author: Cletus Olisenekwu Email: cletusolisenekwu21@gmail.com



DOI:10.62110/sciencein.mns.2025.v12.1196 URN:NBN:sciencein.mns.2025.v12.1196 O Authors, The ScienceIn https://pubs.thesciencein.org/jmns



Gd is paramagnetic at temperatures higher than 20°C. Its compounds have a long spin relaxation period due to their electrical configuration.<sup>15</sup> In 1880, Jean de Marignac used spectroscopy of the mineral gadolinite to identify gadolinium. In honour of the mineral gadolinite, he gave the element the name Gadolinium. Johan Gadolin, a Swedish/Finnish scientist who found and described this mineral in the 18th century, is honored by the mineral's name. The group of metals known as lanthanides, or lanthanoides, includes gadolinium (Gd), which has atomic number 64, and the 14 elements that follow it in the periodic table, which have atomic numbers 58-71. The group begins with the element lanthanum, which has atomic number 57. oxidation state +3 is adopted by gadolinium in its ionic form in the vast majority of its compounds. [Xe]4f<sup>7</sup>5d<sup>1</sup>6s<sup>2</sup> is a representation of the neutral gadolinium atom's electronic structure. Gd<sup>+3</sup> forms bonds with the 6s<sup>2</sup> and 5d<sup>1</sup> electrons in its ionic state. The significant paramagnetic effect is explained by the seven unpaired electrons in the 4f spherically symmetric orbital.15

Rare-earth elements (RE) are widely used in displays, lasers, optics, and fibre-optic telecommunication systems, temperature sensors, LED phosphors, and optoelectronics because of their photoluminescent (PL) properties. 16-18 Both down and upconversion processes were able to use 4f-4f transitions due to their wide spectral range and variation. Furthermore, lanthanidebased phosphors are very promising materials for opticalelectronic and photovoltaic systems. Gd can be doped with other rare-earth elements to create effective phosphors that emit in the visible and ultraviolet spectrum, which can be used in optoelectronics, sensors, and other luminescence applications. 19,20

Atomization technology has been widely used over the past 20 years and has significantly impacted a number of industries, including manufacturing, chemistry, electronics, energy, agriculture, and pharmacy.21 Although there is a long list of atomization techniques, the electrostatic-spray atomizer is one of the most effective due to its uniform distribution of spayed nanoparticles, its ability to control or modify particle size, which is advantageous for the deposition of thin films, and its high deposition rate, which makes it appropriate for large-area coatings. Other parameters, such as temperature and deposition time, can also be adjusted for the ideal fabrication of thin films. Breaking droplets with an external force produced by an electric field is known as electrostatic spray. Jets of various shapes will emerge from the meniscus at the nozzle when the liquid is subjected to an electric field force that is strong enough. To fragment into smaller droplets, the charged liquid experiences nonuniform fission and ellipsoidal deformation.<sup>22</sup>

The electrostatic spray atomizer, as a microfluidic technology, has been shown to be a potent instrument, allowing for precise control through the manipulation of fluidic materials over certain parameters. As a result, a wide range of technological advancements and applications for electrostatic spray atomization are anticipated. Related applications have been growing quickly in tandem with the theoretical study of electrostatic spray becoming more in-depth. There is,

nevertheless, an ongoing and expanding promise. An emerging technology that expands the range of applications for nanomaterials is the ability of electrostatic spray devices to produce droplets with a size distribution as small as the nanometer level.<sup>21</sup>

Dopants are known to try to alter the electrical, optical, and electronic characteristics of semiconducting materials.<sup>23–26</sup> By adding an impurity in a quantum-confined structure, the main pathway for recombination from surface states to impurity levels can be transferred.<sup>27</sup> The energy band gap of a semiconductor material affects the operational wavelength of an optoelectronic device. Realizing any desired band gap, or even spatially graded band gaps, is essential for applications such as detectors, LEDs, solar cells, and lasers. Unlike most electrical devices, which are based on silicon, III-V semiconductor materials and their alloys are widely employed to construct optoelectronic devices since they have a direct band gap.<sup>28–31</sup>

The advancement of photonics and optoelectronics relies heavily on developing high-performance thin films with superior electrical conductivity. Chalcogenide nanoparticle thin films, particularly those incorporating zirconium sulphide (ZrS) and gadolinium (Gd), offer promising potential due to their unique electronic and optical properties.<sup>32</sup> However, achieving optimal electrical conductivity in electro-sprayed chalcogenide films remains a critical challenge. This problem arises due to inconsistencies in the deposition process, variations in nanoparticle distribution, and potential defects in film morphology, which affect charge transport mechanisms.<sup>33</sup> To address this problem, an in-depth investigation and optimization of the electrical conductivity properties of ZrS/Gd chalcogenide nanoparticle thin films are necessary. This can be achieved through systematic experimental studies involving controlled electro-spraying parameters, advanced characterization techniques, and post-deposition treatments to enhance charge transport. By optimizing key factors such as spray parameters, precursor concentrations, precursor voltage, and precursor temperature, the electrical conductivity of these films can be significantly improved, making them more suitable for highperformance photonic and optoelectronic applications.

### **MATERIALS**

The materials used for the deposition and characterization of Zirconium sulphide doped with Gadolinium (ZrS/Gd) thin films are; Zirconium (IV) oxychloride octahydrate (ZrOCl<sub>2</sub>.8H<sub>2</sub>O), Gadolinium Oxide (Gd<sub>2</sub>O<sub>3</sub>), Thioacetamide (C<sub>2</sub>H<sub>5</sub>NS), hydrochloric acid (HCl), distilled water, Heating mantle, Power supply, Fluorine doped tin oxide as substrate (FTO), A digital weighing balance, Digital hand-held pH meter (HL7300) with a pH value of 7.0, Magnetic stirrer, Stopwatch, Voltmeter, Digital multimeter, Ammeter, Thermometer 0-500°C, Electrostatic Spray Atomization, UV-1800 Visible Spectrophotometer, Bruker D8 Advance X-ray diffractometer with Cu-K $\alpha$  line ( $\lambda$  = 1.54056 Å) in 2 $\theta$  range from 10° - 90°, Four point probe (Model T345) and Scanning Electron Microscopy.

### **METHODS**

The Electrostatic Spray Deposition technique (ESD) was used in this research. It refers to breaking droplets using an external force caused by an electric field. A sufficient electric field force was applied to the solution of ZrS/Gd, and jets of different shapes were emitted from the meniscus at the nozzle. The charged solutions or liquids underwent ellipsoidal deformation and nonuniform fission to break down into smaller droplets. Electrostatic spray, as a microfluidic technology, is a powerful tool with precise control gained by manipulating fluidic materials over some parameters. The electrostatic spray system is composed of a source of the cation, i.e., Zirconium (IV) oxychloride octahydrate (ZrOCl<sub>2</sub>.8H<sub>2</sub>O), a source of the anion, i.e., Thioacetamide (C<sub>2</sub>H<sub>5</sub>NS), and distilled water. The power supply was used to provide an electric field containing the solutions to the fluorine-doped tin oxide as substrate (FTO). Finally, uniform deposition of thin films by the electrostatic spray deposition technique was achieved.

### 3.1 Substrate Cleaning Procedure

Conducting glass served as the substrate. After dipping the substrates in methanol and acetone, they were washed with distilled water and then ultrasonically sonicated in an acetone solution for 30 minutes. After that, they were cleaned with distilled water and allowed to dry in an oven.

### **RESULTS**

## 4.1 Optical Study of Zirconium Sulphide and Zirconium Sulphide Doped Gadolinium (ZrS/Gd)

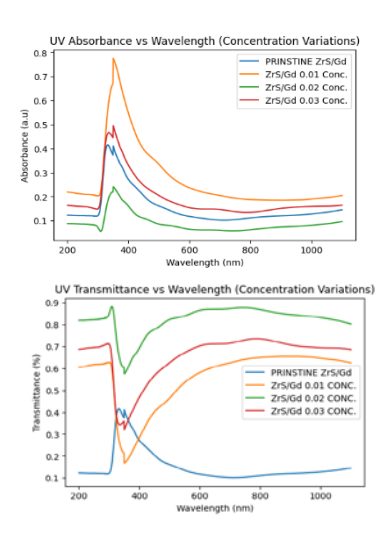


Figure 1. (a) Absorbance, (b) Transmittance, and (c) Reflectance vs Wavelength

Plots of the absorbance, transmittance, and reflectance of gadolinium-doped ZrS and undoped ZrS are shown in Figure 1 for various deposition concentrations between 0.01 to 0.03 mol. The graph, Figure 1(a) shows UV absorbance vs. wavelength for different ZrS/Gd concentrations. A strong absorbance peak is observed around 300–400 nm, with intensity decreasing as concentration increases, except for 0.01 Conc., which has the highest absorbance of 0.75a.u. This shows concentration-

dependent optical properties, due to aggregation or structural changes. The decreasing trend beyond 400 nm indicates reduced light absorption in the visible range.<sup>34</sup> Figure 1 is the UV-Vis reflectance spectra of ZrS/Gd with different concentrations. From the graph, there is an intense reflectance peak at approximately 300–400 nm with variable intensity by concentration. In general, the higher the concentration, the lower the reflectance, which means higher absorption. The reflectance decreases steadily above 400 nm with certain oscillations at longer wavelengths. The trend indicates the effect of doping concentration on the optical properties of ZrS/Gd, which plays an important role in applications in the area of photonics and energy materials such as photodiodes, phototransistors, photonic integrated circuits, electro-optic modulators, etc.<sup>28</sup> Figure 1(c) illustrates the wavelength and UV transmittance for different concentrations of ZrS and ZrS/Gd. The pristine sample of ZrS has the lowest transmittance, meaning that it absorbs more UV light compared to the doped samples. Transmittance increases when the concentration of ZrS/Gd is increased, particularly in the visible and near-infrared regions. A sharp transmittance reduction in the 250-400 nm range signifies intense UV absorption, which suggests efficient blocking of UV radiation by the material. Transmittance rises and levels off beyond this range, with the sample's 0.02 and 0.03 concentrations being the most transparent. This shows that there is improved optical transparency when the ZrS/Gd concentration is higher, proving to be useful for application in UV filters, optical coatings, or solar energy devices.

# 4.2. Tauc Study of ZrS and ZrS/Gd Material Deposited at Different Dopant Concentrations for Photonic-Optoelectronic Devices

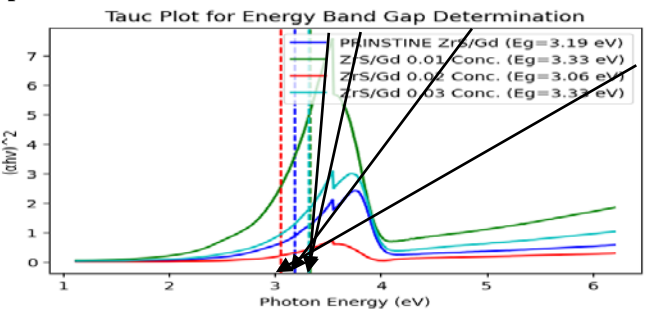
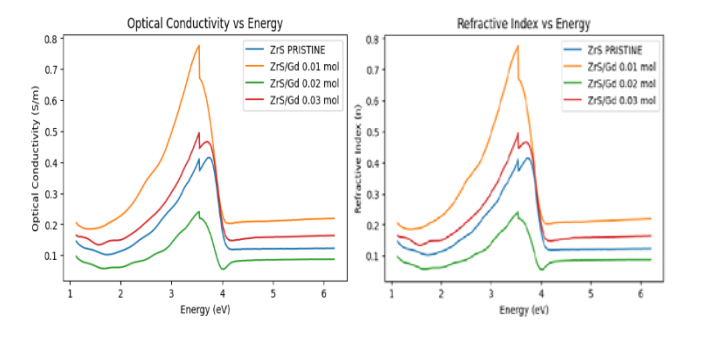


Figure 2. Absorption Coefficient Square Vs Photon Energy

The Tauc's plot presented in Figure 2 is the optical band gap estimation applied to the different ZrS/Gd concentrations studied, and also to the pristine sample, which obeys the same Tauc relation to calculate the band gap. The vertical dashed lines represent the extrapolated energy band gap for the samples. The pure sample for ZrS/Gd has a band gap of around 3.19 eV. The results showed the dependence of band gaps on the cation concentration, where the concentrations of Gd = 0.01 and 0.03 showed higher band gaps of about 3.33 eV. The differences in band gap values specify the evolution of material composition and defects or quantum confinement effects as a result of Gd

doping. The fact that the band gaps are broad and their quantities are over 3 eV effectively shows that there is high absorption in the UV-spectra, and such materials could be effectively utilized for the UV photodetectors and solar-blind sensors, antireflective materials, UV light-emitting diodes and laser applications.<sup>1</sup>



**Figure 3.** (a) Optical Conductivity, and (b) Refractive Index Vs Photon Energy

Plots of optical conductivity and refractive index vs photon energy of gadolinium-doped ZrS and undoped ZrS are shown in Figure 3 for various deposition concentrations between 0.01 to 0.03 mol. The graph (Figure 3a) shows the variation of optical conductivity (S/m) with energy (eV) for different compositions of ZrS (Zirconium Sulphide) doped with Gd (Gadolinium) at different molar concentrations. The pristine ZrS sample exhibits a moderate increase in conductivity with energy, peaking around 3.8 eV before dropping. The doped samples show distinct variations, with ZrS/Gd 0.01 mol exhibiting the highest peak conductivity (~0.75 S/m), followed by 0.03 mol and 0.02 mol doped samples. The peak optical conductivity shifts slightly with doping concentration, indicating changes in electronic transitions and band structure modifications due to Gd incorporation. The trend shows that doping influences charge carrier concentration and transition probabilities, with higher doping levels affecting the optical response more significantly. The concentration-based variations could be used for the design of sensitive optoelectronic devices such as tunable light-emitting diodes thermoelectric generators, etc.

Figure 3(b) shows the variation of the refractive index (n) as a function of energy (eV) for pristine ZrS and Gd-doped ZrS at different doping concentrations (0.01 mol, 0.02 mol, and 0.03 mol). The refractive index exhibits a peak around 3-4 eV, indicating strong optical transitions in this energy range. The pristine ZrS sample has a moderate refractive index, while the 0.01 mol Gd-doped ZrS shows the highest peak, confirming enhanced optical response due to doping. However, at 0.02 mol, the refractive index drops significantly, indicating possible structural changes or absorption effects reducing optical response. The 0.03 mol sample shows an intermediate behaviour between 0.01 mol and pristine ZrS, showing a nonlinear relationship between doping concentration and optical properties. The trend indicates that controlled Gd doping can tune the refractive index of ZrS, making it useful for optoelectronic and photonic applications.<sup>35</sup>

## 4.3 The Resistivity and Conductivity Study of ZrS and Gadolinium Doped Zirconium Sulphide (Gd: ZrS)

The table below details the resistivity and conductivity parameters of Gd-doped ZrS films under varying dopant concentrations to evaluate conductivity behaviour.

**Table 1**: Electrical Properties of Zirconium Sulphide (ZrS) and Zirconium Sulphide (ZrS) Doped Gadolinium at Various Dopant Concentrations for Photonic-Optoelectronic Applications.

Samples	Thickness (nm)	Resistivity (Ω.m)	Conductivity (S/m) <sup>-1</sup>
ZrS (Pristine)	101.99	0.60584371	1.65059071
ZrS/Gd 0.01 mol	108.29	0.57059747	1.752548956
ZrS/Gd 0.02 mol	110.22	0.560606061	1.783783784
ZrS/Gd 0.03 mol	114.02	0.54192247	1.845282408

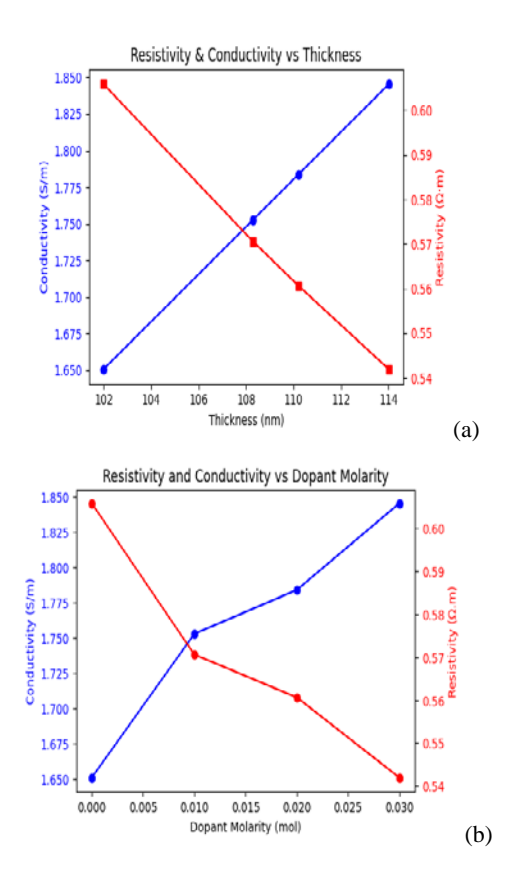


**Figure 4**. (a) Resistivity, Conductivity vs Thickness and (b) Resistivity, Conductivity vs Dopant Molarity.

The graph (Figure 4a) shows an inverse relationship between resistivity and conductivity. As the thickness increases from approximately 102 nm to 114 nm, conductivity increases steadily, while resistivity decreases. This trend aligns with the fundamental principle that conductivity and resistivity are

reciprocals of each other. The blue markers indicate a rising trend in conductivity, showing that increased thickness enhances electron transport, due to reduced scattering effects or improved structural continuity. Conversely, the red markers show a consistent drop in resistivity, reinforcing the idea that thicker films offer lower resistance to electrical flow. This behaviour is typical in doped thin films, where enhanced material deposition improves conductive pathways. The observed trend in the graph effectively shows that increasing film thickness enhances conductivity while reducing resistivity, which is beneficial for several optoelectronics applications, including touchscreens, OLED displays, and solar cells.

The graph Figure 4(b) shows a clear inverse correlation between conductivity and resistivity as the dopant molarity increases. Initially, at 0.000 mol, the material exhibits high resistivity and low conductivity. As the dopant concentration increases to around 0.010 mol, the resistivity drops sharply while conductivity rises, indicating enhanced charge carrier density due to doping. Beyond this point, resistivity continues to decrease at a slower rate, while conductivity increases steadily, reaching its highest value at 0.030 mol. This behaviour implies that doping effectively improves electrical transport by reducing scattering and increasing free charge carriers. However, an optimal doping level must be maintained, as excessive doping can lead to defects or saturation effects that may alter the material's performance. This result is paramount in applications such as semiconductors, transparent conductive films, and optoelectronic devices such as diodes, LEDs, etc., where controlled conductivity is essential.

## 4.4 Structural Study of ZrS and Gadolinium Doped Zirconium Sulphide (Gd: ZrS)

The X-ray diffraction (XRD) patterns in Figure 5 show the structural analysis of ZrS doped with varying concentrations of Gd (Gadolinium), ranging from pristine ZrS (undoped) to 0.01 mol, 0.02 mol, and 0.03 mol dopant levels. The diffraction peaks are labelled with their corresponding Miller indices (hkl): (111), (211), (112), and (200), indicating crystalline phases. For the pristine ZrS sample, the most intense peak is observed at approximately  $2\theta \approx 28^{\circ}$ , corresponding to the (111) plane, with other prominent peaks around 32°, 40°, and 50° indexed as (112), (200), and (211), respectively. As the Gd concentration increases to 0.01, 0.02, and 0.03 mol, respectively, there is a noticeable shift in peak intensity and sharpness. The 0.01 mol and 0.02 mol samples retain similar peak positions but show reduced intensity and slight broadening, indicating lattice strain or reduced crystallinity due to Gd incorporation. The 0.03 mol sample exhibits the broadest peaks and lowest intensity, especially for the (112) and (200) planes, showing a significant structural distortion or decreased crystal quality at higher doping levels. The observed peak shifting and broadening indicate that Gd ions have been successfully incorporated into the ZrS lattice, either by substituting for Zr atoms or occupying interstitial positions, resulting in slight changes to the crystal structure. These structural changes can enhance the material's electrical, magnetic, or catalytic properties, making it suitable for applications in photocatalysis, optoelectronics, and energy

Table 2: ZrS/Gd XRD Result for Concentration Variations

Sam	2θ	Spacing	Lattice	FWH	Crystall	Dislocatio
ple	(degree	d		M (°)	ine	n
	s)	(Å)	Constant a (Å)		Size D (nm)	Density (1/nm²)
ZrS Prist ine	15	5.90149 7522	5.901497 522	0.1	801.283 9969	1.5575E- 06
	15.0343	5.88811 063	5.888110 63	0.1	801.315 6101	1.55737E- 06
	15.0686	5.87478 4858	5.874784 858	0.1	801.347 2975	1.55725E- 06
ZrS/ Gd 0.01 mol	15	5.90149 7522	5.901497 522	0.5	160.256 7994	3.89374E- 05
	15.0343	5.88811 063	5.888110 63	0.45	178.070 1356	3.15368E- 05
	15.0686	5.87478 4858	5.874784 858	0.4	200.336 8244	2.4916E- 05
ZrS/ Gd 0.02 mol	15	5.90149 7522	5.901497 522	0.5	160.256 7994	3.89374E- 05
	15.0343	5.88811 063	5.888110 63	0.45	178.070 1356	3.15368E- 05
	15.0686	5.87478 4858	5.874784 858	0.4	200.336 8244	2.4916E- 05
ZrS/ Gd 0.03 mol	15	5.90149 7522	5.901497 522	0.5	160.256 7994	3.89374E- 05
	15.0343	5.88811 063	5.888110 63	0.45	178.070 1356	3.15368E- 05
	15.0686	5.87478 4858	5.874784 858	0.4	200.336 8244	2.4916E- 05

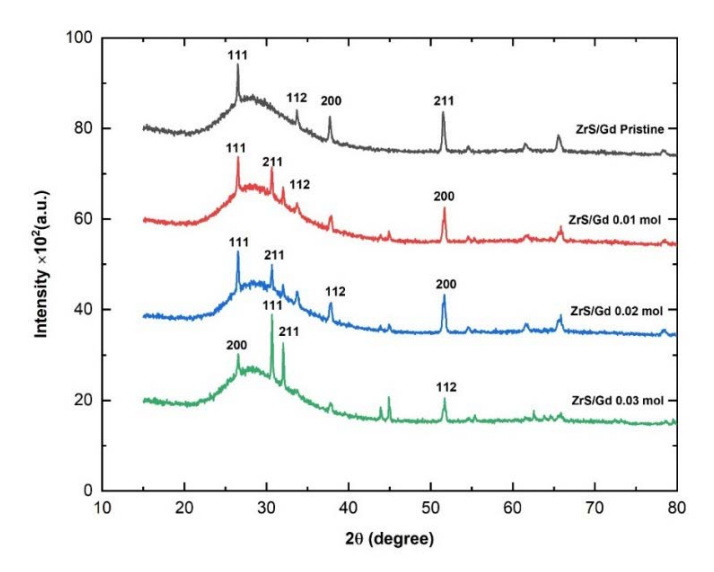


**Figure 5**: XRD Study of ZrS and ZrS Doped Gadolinium (ZrS/Gd) at Various Dopant Concentrations.

storage. Among the samples, the one with  $0.01\ mol\ Gd$  shows an optimal balance between maintaining crystallinity and benefiting

from dopant-induced effects, making it ideal for applications that require moderate structural modification.

Table 2 includes additional characteristics and the crystallite size of the films, in addition to the computed crystallite or grain sizes, dislocation density, and dopant molarity for the films deposited at various gadolinium dopants were estimated using equations (1–4):

$$D = k\lambda/\beta \cos\theta \tag{1}$$

$$d = \lambda / 2 \sin \theta \tag{2}$$

$$a = d\sqrt{h^2 + k^2 + l^2} \tag{3}$$

$$\delta = 1/D \tag{4}$$

## 4.5 Surface Morphology of ZrS and Gadolinium Doped Zirconium Sulphide (Gd/ZrS)

Surface Morphology and Graphical Presentation of ZrS and ZrS Doped Gadolinium at Various Dopant Concentrations.

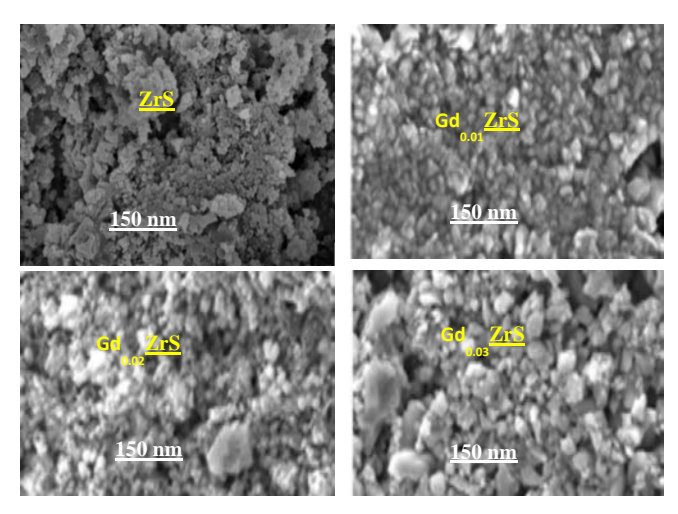
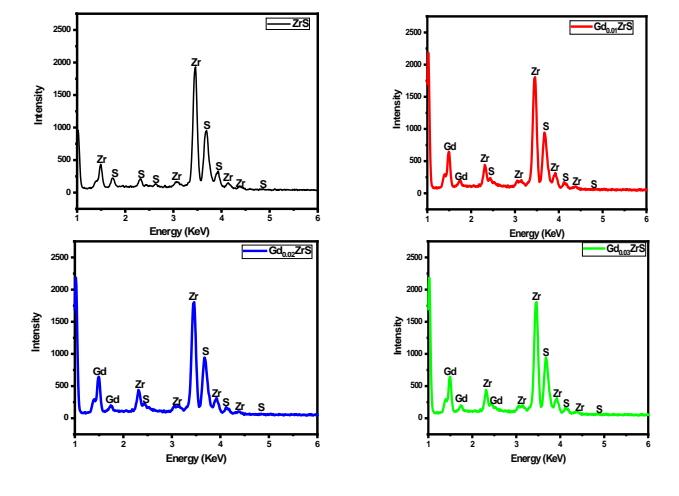


Figure 6: SEM Micrograph.



**Figure 7**: Elemental Spectrum of ZrS and Gadolinium Doped Zirconium Sulphide (ZrS/Gd).

The ZrS and gadolinium-doped zirconium sulphide (ZrS/Gd) micrograph in Figure 6 shows agglomeration on the films with large grain size, or nanoparticles, and no pinholes. The morphology of the ZrS surface shows a Clove-like surface with precipitate apparent in the ZrS micrograph; the substrate's large grain size shows photon absorption but no pinholes. The ZrS precursor underwent a significant alteration upon the addition of gadolinium as a dopant, as seen in the surface micrograph of the films under analysis. There was a cloud-like precipitate that was visible on the film's surface morphology. For the material deposited at 0.03 mol, the cloudlike precipitate gradually cleared off as the dopant concentration rose, forming a dense cloud in one area of the surface. For optoelectronic-photonic applications, the doped ZrS material demonstrated uniform deposition of nanoparticles covering the entire substrate. They will be a strong contender for optoelectronic-photonic and other applications in the electronics and communication sectors because the surface micrograph of the gadolinium-doped films is well-structured on the surface of the FTO substrate used for the synthesis, without any cracks or lattice strain. The elemental spectrum of ZrS and gadolinium-doped ZrS films is shown in Figure 7. Zirconium sulfide and the dopant gadolinium are seen as strong peaks in the spectrum.

### CONCLUSION

This study successfully demonstrates that doping Zirconium Sulphide (ZrS) thin films with Gadolinium (Gd) significantly enhances their optoelectronic properties, making them excellent candidates for high-performance applications. Optical analysis revealed increased UV absorbance and improved transmittance with higher Gd concentrations, while the bandgap values increased from 3.19 eV (undoped) to 3.33 eV at 0.01 and 0.03 mol, signifying better UV light interaction. Electrical conductivity increased steadily from 1.65 S/m (pristine) to 1.85 S/m at 0.03 mol, while resistivity decreased from 0.61  $\Omega$ ·m to 0.54 Ω·m. Structural analysis via XRD confirmed crystallite size enhancement and reduced dislocation density, indicating improved material quality with doping. SEM imaging revealed uniform and agglomerated nanoparticle deposition without cracks or pinholes, suggesting a robust surface morphology suitable for device integration. These findings show that the electrostatic spray technique, combined with controlled Gd doping, can effectively tune the optical and electrical performance of ZrS films, positioning them as promising materials for advanced optoelectronic and photonic technologies.

### CONFLICT OF INTEREST STATEMENT

Authors declare that there is no conflict of interest for this work.

### REFERENCES AND NOTES

- S. Nazir, J.M. Zhang, M. Junaid, et al. Metal-based nanoparticles: Basics, types, fabrications and their electronic applications. *Zeitschrift fur Phys. Chemie* 2024, 238 (6), 965–995.
- A. Bouafia, S.E. Laouini, A.S.A. Ahmed, et al. The recent progress on silver nanoparticles: Synthesis and electronic applications. *Nanomaterials* 2021, 11 (9), 2318.

- N. Hossain, M.H. Mobarak, M.A. Mimona, et al. Advances and significances of nanoparticles in semiconductor applications – A review. *Results Eng.* 2023, 19, 101347.
- 4. S. Khan, M.K. Hossain. Classification and properties of nanoparticles. In *Nanoparticle-Based Polymer Composites*; **2022**; pp 15–54.
- N. Joudeh, D. Linke. Nanoparticle classification, physicochemical properties, characterization, and applications: a comprehensive review for biologists. *J. Nanobiotechnology* 2022, 20 (1), 262.
- Y. Khan, H. Sadia, S.Z. Ali Shah, et al. Classification, Synthetic, and Characterization Approaches to Nanoparticles, and Their Applications in Various Fields of Nanotechnology: A Review. *Catalysts* 2022, 12 (11), 1386.
- R. Hazarika, D. Roy, D. Das, K. Deori. Recent Developments of Nanostructured Photocatalysts Based on Semiconducting Chalcogenides for Organic Reactions. *Curr. Indian Sci.* 2024, 02 (1), 2210299 311728.
- A.S. Mohamed, H. Ahmad. Insight into the electronic, optical, thermodynamic, and thermoelectric properties of novel chalcogenides: An ab initio study. *Int. J. Quantum Chem.* 2024, 124 (1), 27309.
- I. Venditti. Gold nanoparticles in photonic crystals applications: A review. Materials (Basel). 2017, 10 (2), 97.
- M.S. Rider, Á. Buendía, D.R. Abujetas, et al. Advances and Prospects in Topological Nanoparticle Photonics. ACS Photonics 2022, 9 (5), 1483– 1499.
- A. Sosna-Głębska, N. Szczecińska, K. Znajdek, M. Sibiński. Review on metallic oxide nanoparticles and their application in optoelectronic devices. *Acta Innov.* 2019, 30 (30), 5–15.
- K. V. Chandekar, M. Shkir, A. Khan, et al. Significant and systematic impact of yttrium doping on physical properties of nickel oxide nanoparticles for optoelectronics applications. *J. Mater. Res. Technol.* 2021, 15, 2584–2600.
- A. Rahman, M.M. Khan. Chalcogenides as photocatalysts. *New J. Chem.* 2021, 45 (42), 19622–19635.
- M.M. Khan. Introduction and fundamentals of chalcogenides and chalcogenides-based nanomaterials. *Chalcogenide-Based Nanomater. as Photocatal.* 2021, 1–6.
- L. Blomqvist, G.F. Nordberg, V.M. Nurchi, J.O. Aaseth. Gadolinium in Medical Imaging—Usefulness, Toxic Reactions and Possible Countermeasures—A Review. *Biomolecules* 2022, 12 (6), 742.
- M.K. Hossain, S. Hossain, M.H. Ahmed, et al. A Review on Optical Applications, Prospects, and Challenges of Rare-Earth Oxides. ACS Appl. Electron. Mater. 2021, 3 (9), 3715–3746.
- Z. Chen, G. Dong, G. Barillaro, J. Qiu, Z. Yang. Emerging and perspectives in microlasers based on rare-earth ions activated micro-/nanomaterials. *Prog. Mater. Sci.* 2021, 121, 100814.
- S. Singh, D. Singh, P. Siwach, I. Gupta, P. Kumar. Synthesis Strategies for Rare Earth Activated Inorganic Phosphors: A Mini Review. *Appl. Res.* 2025, 4 (1), 0190.
- A. Ćirić, S. Stojadinović. Photoluminescence of Gd2O3 and Gd2O3:Ln3+ (Ln = Eu, Er, Ho) formed by plasma electrolytic oxidation of pure gadolinium substrate. Opt. Mater. (Amst.). 2020, 99, 109546.
- P. Singh, S. Kachhap, P. Singh, S.K. Singh. Lanthanide-based hybrid nanostructures: Classification, synthesis, optical properties, and multifunctional applications. *Coord. Chem. Rev.* 2022, 472, 214795.

- J. Wang, Y. Zhang, W. Zhang, Z. Fan. Research Progress of Electrostatic Spray Technology over the Last Two Decades. *J. Energy Eng.* 2021, 147 (4), 3121003.
- 22. X. Zhu, Q. Zhang, Y. Wang, F. Wei. Review on the nanoparticle fluidization science and technology. *Chinese J. Chem. Eng.* **2016**, 24 (1), 9–22.
- I.L. Ikhioya, A.C. Nkele, D.N. Okoli. Effects of temperature and ph variations on electrochemically-deposited zirconium-doped zinc selenide thin films. Optik (Stuttg). 2022, 260 (September 2021), 169055.
- A.Y. Yassin. Synthesized polymeric nanocomposites with enhanced optical and electrical properties based on gold nanoparticles for optoelectronic applications. J. Mater. Sci. Mater. Electron. 2023, 34 (1), 46.
- E.O. Ojegu, S.O. Samuel, M.O. Osiele, G.E. Akpojotor, I.L. Ikhioya. Optimisation of deposition voltage of zirconium-doped chromium telluride via typical three-electrode cell electrochemical deposition technique. *Mater. Res. Innov.* 2024, 28 (3), 137–145.
- I.L. Ikhioya, A.C. Nkele, S.N. Ezema, M. Maaza, F. Ezema. A study on the effects of varying concentrations on the properties of ytterbiumdoped cobalt selenide thin films. Opt. Mater. (Amst). 2020, 101, 109731.
- I.L. Ikhioya, A.J. Ekpunobi. Effect of Deposition Period and pH on Electrodeposition Technique of Zinc Selenide Thin Films Materials and Methods Results and Discussion Optical Properties of ZnSe Films. *J. Niger. Assoc. Math. Phys.* 2014, 28 (2), 281–288.
- S.O. Samuel, F.E. James, J.T. Zhimwang, et al. Effect of dopant on the energy bandgap on strontium sulphide doped silver for optoelectronic application. *Mater. Res. Innov.* 2024, 28 (1), 8–18.
- A.I. Abdel-Salam, M.M. Awad, T.S. Soliman, A. Khalid. The effect of graphene on structure and optical properties of CdSe nanoparticles for optoelectronic application. *J. Alloys Compd.* 2022, 898, 162946.
- P. Kumar, S. Singh, I. Gupta, et al. Structural refinement and optical characteristics of single-phase Gd3Al5O12:Er3+ nanophosphors for luminescent applications. J. Lumin. 2022, 252, 119338.
- S. Singh, D. Singh. Structural and optical properties of green emitting Y2SiO5:Tb3+ and Gd2SiO5:Tb3+ nanoparticles for modern lighting applications. *Rare Met.* 2021, 40 (11), 3289–3298.
- 32. O.S. Shaka, C. Olisenekwu, I.L. Ikhioya. Analyzing the structural, optoelectronic, and optical properties of ZrS nanostructured material by adding silver (Ag) dopant to its lattice. *Niger. J. Sci. Environ.* **2024**, 22 (3), 74–90.
- S. Ibrar, E.O. Ojegu, O.B. Odia, et al. Assessing High-Performance Energy Storage of the Synthesized ZIF-8 and ZIF-67. *J. Appl. Organomet. Chem.* 2023, 3 (4), 294–307.
- M. Othmane, A. Attaf, F. Bouaichi, H. Saidi. An approach to the description of the correlation between the electrical conductivity and the band gap of F-doped zinc oxide thin films. *J. Mater. Sci. Mater. Electron.* 2025, 36 (2), 119.
- S.O. Samuel, E.O. Ojegu, I.L. Ikhioya. Investigating the Impact of Voltage on Optoelectronic Features of Silver Incorporated into the Lattice of Zirconium Sulphide Nanostructured Material. *Phys. Access* 2024, 04 (02), 126–138.